The Gray Institute Open Microscopes applied to radiobiology and protein interaction studies

PR Barber[1], IDC Tullis[1], MI Rowley[2], CD Martins[1], G Weitsman[3], K Lawler[2], M Coffey[3], N Woodman[6], CE Gillett[5,6], T Ng[3,4,5], B Vojnovic[1,4]

[1]Gray Institute for Radiation Oncology and Biology, Department of Oncology, University of Oxford, UK
[2]Institute for Mathematical and Molecular Biomedicine, King's College London, UK
[3]Division of Cancer Studies, King's College London, UK
[4]Randall Division, King's College London, UK
[5]Breakthrough Breast Cancer Research Unit, King's College London, London, UK
[6]Guy's & St Thomas' Breast Tissue & Data Bank, King's College London, Guy's Hospital, London, UK

ABSTRACT

We describe an 'open' design methodology for wide-field fluorescence, confocal and fluorescence lifetime imaging microscopy (FLIM), and how the resulting microscopes are being applied to radiation biology and protein activity studies in cells and human tissue biopsies. The design approach allows easy expansion as it moves away from the use of a monolithic microscope body to small, commercial off-the-shelf and custom made modular components. Details have been made available under an open license for non-commercial use at http://users.ox.ac.uk/~atdgroup.

Two radiobiology 'end-stations' have been constructed which enable fast radiation targeting and imaging of biological material opening up completely novel studies, where the consequences of ionising radiation (signaling and protein recruitment) can be studied *in situ*, at short times following irradiation. One is located at Surrey University, UK, where radiation is a highly focused in beam (e.g. protons, helium or higher mass ions). The second is installed at the Gray Institute linear accelerator facility, Oxford University, which uses sub-microsecond pulses of 6 MeV electrons.

FLIM capabilities have enhanced the study of protein-protein interactions in cells and tissues via Förster Resonance Energy Transfer (FRET). Extracting FRET signals from breast cancer tissue is challenging because of endogenous and fixation fluorescence; we are investigating novel techniques to measure this robustly. Information on specific protein interactions from large numbers of patient tumors will reveal prognostic and diagnostic information.

1. INTRODUCTION

We recently published an open microscope design methodology together with details of microscopes built using this approach[1]. This methodology is a flexible and affordable way to build bespoke microscopes in the laboratory setting that can be automated and incorporate the latest advanced imaging methods. Of the 7 microscopes built to date 3 offer laser-scanning confocal as well as wide-field fluorescence imaging techniques and have been extended to include fluorescence lifetime imaging microscopy (FLIM). The design approach allows easy expansion as it moves away from the use of a monolithic microscope body to small, commercial off-the-shelf and custom made modular components. Details have been made available under an open license for non-commercial use at http://users.ox.ac.uk/~atdgroup. This type of customization and flexibility has great benefit in the research environment where novel experiments are often 'evolving' and the microscope system cannot be a 'black-box' to staff on-site. Novel aspects such as scriptable time-lapse actions (in the Python programming language), the ability to control ancillary, and often very complex, equipment within the same software environment and important details to allow quantitative microscopy (e.g. excitation power monitoring of every wide-field or laser scanned image) have also been added. In this paper we present brief details of how variants of these microscopes have been used as radiation endstations (Section 2) as well as further developments for detecting protein interactions in tissue via lifetime-based tissue segmentation (Section 3).

2. APPLICATION TO RADIOBIOLOGY STUDIES

2.1 The University of Oxford LINAC Endstation

Although much is understood about repair processes in mammalian cells following irradiation[2,3,4] some details, and in particular, the kinetics of specific repair processes are still poorly understood. Following absorption of ionizing radiation, various types of damage to the cell take place, including single-strand breaks, double-strand breaks and clustered type of damage in the cell nuclear DNA. Mammalian cells have evolved numerous repair mechanisms to counteract this damage, but the studies of the sequence of the signaling events are sometimes hampered by the lack of instrumentation able to determine *in situ* the various pathways involved in the repair process (or otherwise). Furthermore, the ability to interfere with these pathways may form the basis for modifying the cell's response to ionizing radiation. Low Linear Energy Transfer (LET) radiation is of particular interest as this type of radiation is the most commonly used for radiotherapy treatment (MeV electron and photon beams).

One approach to study these processes is to combine a low LET source with a research-grade fluorescence microscopy platform. This approach poses significant logistic problems due to (1) the fact that modern microscope bodies cannot be easily adapted to operate in a radiation environment (2) the formation of color centers in glasses[5,6] used in the various lenses in the microscope optical system. Both of these limitations are overcome by utilizing our 'open' microscope design approaches, by using appropriate radiation shielding near critical components and by enhancing the microscope with a sample transport system: this moves cell irradiation vessels between irradiation and imaging stations (http://users.ox.ac.uk/~atdgroup/radiation_linac.shtml). In our arrangement, the low LET radiation source is a reconditioned 6 MeV linear accelerator, modified to produce single, rather than repetitive, pulses of electrons over pulse widths of 25 ns-1 μs. These 6 MeV electron pulses irradiate sideways a small coverslip-bottomed square dish where the cells are plated. An X-Z programmable motion control system is used to transport the dishes (Figure 1) and works in

synchrony with the radiation source and the fluorescence microscope, as it is programmed within the same environment described by Barber et al.[1] The microscope, storage area and various radiation dose monitoring devices are enclosed in an incubator. The temperature and gas concentration within this are regulated to typically 37 degC and 5% CO_2, an environment appropriate for cell time-lapse imaging. Such imaging can be programmed to take place over several hours, with a non-linear time course. This arrangement allows us to study the timescales of the formation and disappearance of numerous proteins, modified by the incorporation of fluorescent proteins[7,8,9].

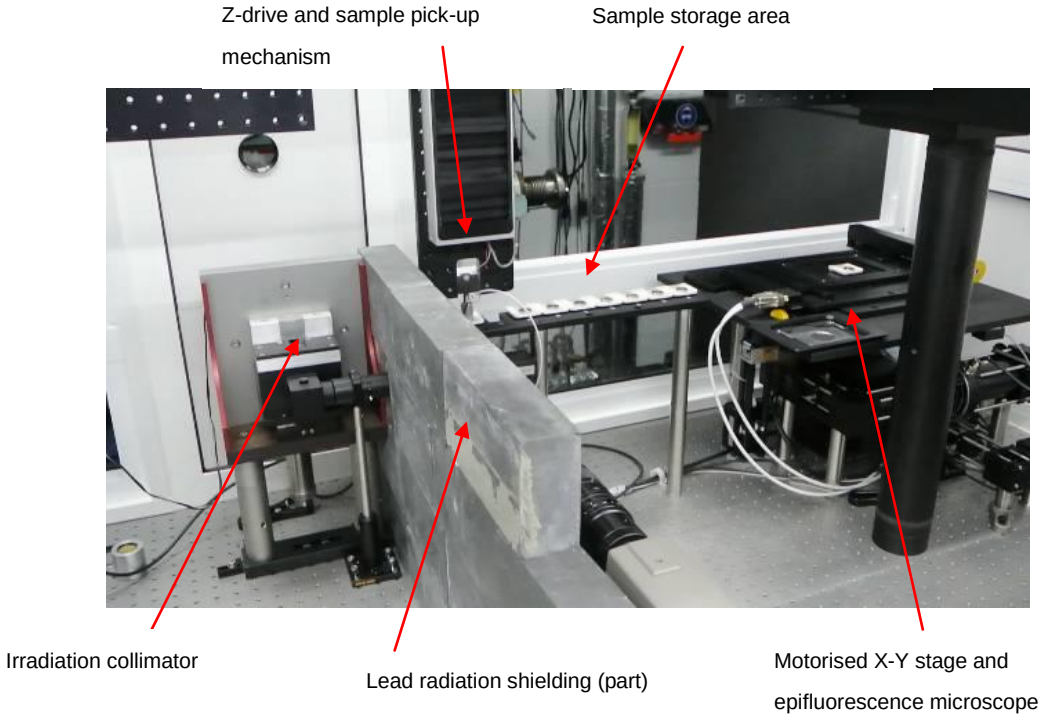

Figure 1. The low LET cell irradiation facility. Lead shielding between the stage and motorized microscope has been removed for clarity. 6 MeV electrons are fired through the irradiation collimator ('out of the page'). Several samples can be picked up by the Z-drive mechanism from the sample storage are and moved to and from irradiation collimator and microscope positions, using a horizontal X-drive system (not shown).

2.2 The University of Surrey ion beam Endstation

The understanding of cell responses to high LET ionizing radiations such as α-particles and high-energy ions is also important[10,11,12]. Environmental exposures, recent radiotherapy advances bases on proton and carbon ion irradiations and space research are some of the fields that require studies of biological responses to such heavily ionizing radiations. Very tight beams (microbeams, ~1-5 μm) of energies of a few MeV have been used in the past for this purpose. Such beams only penetrate ~1 mm or so and it is thus readily possible to couple such sources to microscope optics. However, once again, a 'standard' microscope body is generally not suitable: microscope condenser optics are 'in the way', occupying the physical space required by the ion beam delivery system. Although dedicated systems have been used in the past[13,14,15] a much more flexible approach is provided by coupling a focused, scanned ion beam[16,17] to an arrangement based on the 'open microscope' approach described before[1], and shown in Figure 2.

In this case the software programming environment is extended to include control of (a) an additional piezoelectric stage focus arrangement, so as to be able to bring target cells to the ion beam focus, independently of optical focus, (b) a fast electrostatic beam switch, so as to be able to control delivered dose, (c) particle counting detectors and (d) various functions which control the accelerator which provides the charged particles. This is a Tandem electrostatic accelerator[18] capable of accelerating a wide range of masses. More detailed descriptions of this arrangement have already been published[19]. Although the end-stations described above currently do not include fluorescence lifetime detection, this will undoubtedly be required in the future and its addition will benefit from the advances in lifetime analysis described below.

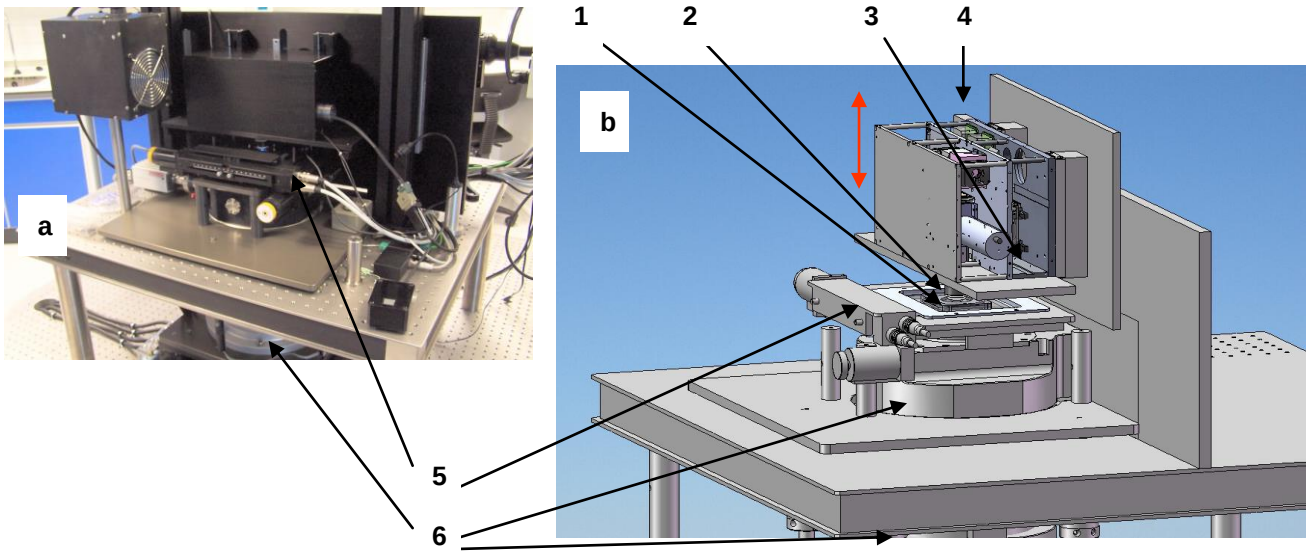

Figure 2. The ion beam/microscopy end-station at the University of Surrey Ion Beam Centre, with a vertical ion beam entering the end-station from below. a: Practical implementation. b: SolidWorks™ model of the assembly, comprising of: 1: biological sample insert; 2: water dipping microscope objective; 3: Optics assembly containing switching devices, optical filters, fluorescence cubes etc.; 4: The complete optical systems moves vertically to allow sample insertion, while the infinity optics tube lens remains fixed in the rear vertical plate; 5: motorized XYZ stage; 6: ion beam focusing quadrupole triplet. The whole arrangement is normally enclosed by an environmental chamber to maintain a 5% CO_2 atmosphere at 37 degC.

3. APPLICATION TO PROTIEN INTERACTION STUDIES IN TISSUES

3.1 Fluorescence Lifetime Imaging and Förster Resonance Energy Transfer

Fluorescence Lifetime Imaging Microscopy (FLIM) and Förster Resonance Energy Transfer (FRET) are increasingly becoming key techniques for the study of protein proximity and interactions in live and fixed cells[20,21,22,23]. The occurrence of FRET between two suitable, spectrally distinct, fluorescent molecules involves the non-radiative transfer of energy from the donor to the acceptor molecules. This additional route of energy loss from the donor excited state

causes a reduction in fluorescence lifetime of the donor molecule. Thus FLIM offers a robust and intensity independent method of detecting FRET. Typically in such studies, samples are prepared that contain a mix of the two fluorophores (donor and acceptor) suitably attached to proteins of interest (the 'DA' samples), along with samples that contain the donor alone (the 'D' samples). The control donor lifetime without FRET is measured from the D samples and this is compared to the donor lifetime in the DA samples to derive some measure of the interaction, for example, the FRET Efficiency[21].

One advantageous aspect of our open microscope systems is the ability to incorporate and automate FLIM acquisition in the form of time-correlated single photon counting[24]. This has paved the way for larger protein interaction studies involving large numbers of biological tissue samples and thus automated methods for tissue segmentation and analysis are required. The following sections are concerned with a method for tissue segmentation to improve FRET detection in these circumstances.

3.2 High-content FLIM of clinical tissue

When our attention is turned to detecting FRET in tissue sections the situation becomes complicated, compared to cells *in-vitro*, by the additional fluorescence components that may interfere with our measurement of the FRET signal. These components are either intrinsic to the tissue or may be introduced in the preparation and mounting process but collectively they are often called the 'auto-fluorescence' (AF) signal[25,26,27]. This is a particular problem when using archived tissue embedded in paraffin and the situation maybe somewhat alleviated if fresh/frozen tissue can be used. The preparation of paraffin embedded tissue for use in this kind of work involves many steps (see Methodology) and in optimizing each step, the removal of auto-fluorescence cannot be the only driver and so it's complete removal by protocol optimization is not possible (antibody specificity and target fluorescence intensity are important considerations)[28,29]. Tissue heterogeneity also dictates that these AF components will not be uniform across the tissue as a whole, but may be thought to be constant on the scale of a biological cell (10 – 100 μm, typically over several pixels of the FLIM image). This compounds the problem that the D and DA samples cannot be identical because of tissue variation through the tissue block.

In an ideal world we may capture large numbers of photons from a tissue field of view (FOV) such that we can fully characterize the multi-exponential nature of the tissue at every pixel but because of the danger of photo-bleaching and the requirement to complete the experiment in a reasonable length of time, this cannot be done. Compounded upon this is the need to collect lifetime measurements from small areas of tissue (pixel bins) because of the tissue heterogeneity thus forcing small numbers of photons (100's to 1000's) originating from a multi-exponential response to be analyzed. Thus the most robust method for analysis available to us is to consider the response to be mono-exponential and measure an 'average' lifetime (τ_{ave}), since many more photons are required to use high order exponential models robustly[30,31]. This, however, presents a problem as the average lifetime will be effected by the relative concentrations of the target fluorophore (antibody linked to the tissue protein of interest) and the AF. Changes in concentration could be recorded as false FRET signals if the average AF lifetime is less than the lifetime of the target fluorophore.

3.3 Maximizing the target signal through tissue segmentation

In this and the following sections we present two approaches that may be adopted to avoid AF and maximize the signal

recorded from the target fluorophore and these are compared to the simple intensity thresholding that may be used to include all tissue areas.

Firstly we may consider filtering the pixels (or pixel bins) to only include those which conform well to the mono-exponential model, and are therefore largely free of AF. In the Methodology section we give details of how this can be achieved using the graphical phasor method for exponential analysis[32], by considering those pixels that lie close to the universal circle. This is robust with small photon counts because the mono-exponential model is assumed.

We may also consider those pixel bins that have a dominant contribution due to a component of the expected lifetime of the target fluorophore. With such a 'lifetime filter' we can preferentially select for the target alone or when undergoing FRET through selection of the filter characteristics. We have chosen to use a filter based on a tri-exponential model, where the lifetime components are fixed so that the data fitting problem becomes linear with a reduced number of parameters such that it is robust with small photon numbers.

3.4 Methodology

The methods used to obtain the results in the Results section are detailed in the following subsections.

3.4.1 Lifetime determination

All lifetime fitting was done with the TRI2 software program[33] (versions 2.7.8.10 and above), available from our website (http://users.ox.ac.uk/~atdgroup). The methods used were either based on the Levenberg-Marquardt (LM) algorithm using a maximum likelihood optimizer (MLE)[34]; our C-code has been published online in the Slim Curve fitting library (http://loci.wisc.edu/software/slim-curve) and previously[31], or alternatively based on Bayesian methods to achieve a greater signal to noise ratio[35]. For mono exponential measurements pixels were binned until typically 1,000 counts were in each bin. The regularized inverse Laplace transform algorithm 'rilt' was run in Matlab (http://www.mathworks.co.uk/matlabcentral/ fileexchange/6523-rilt) and was based on the Contin algorithm as published (http://s-provencher.com/pages/ contin.shtml)[36].

3.4.2 Test image preparation

Multi-exponential test images with simulated independent Poisson noise were prepared using the in-house developed program[31] 'TransGenerate' (available from http://users.ox.ac.uk/~atdgroup). The test image used in this paper was designed to simulate a target Alexa fluorophore (lifetime 2.0 – 2.5 ns in DA and D conditions respectively) in tissue with AF (lifetimes 0.25, 1.1 and 3.7 ns, with amplitudes 700, 700, 600 counts per pixel respectively). The two dimensions of the image convey two gradients; horizontally the proportional amplitude of target fluorescence increases from 0 to 90% (left to right), vertically upwards the target fluorophore lifetime decreases from the D condition (2.5 ns) to a FRET DA condition (2.0 ns). This can be seen graphically in Figure 5.

3.4.3 Pixel bin filtering by phasors

To filter the pixel bins which conform well to the mono-exponential model the phasor approach was used. Analytically, the phasor 'trajectory' of a fluorophore undergoing degrees of FRET relative to the universal circle can be plotted as shown in Figure 3[32]. The D and AF points in the figure correspond to the test image and therefore approximate a typical

breast cancer image. The straight line from the 'D' point to the 'AF' point represents a change in concentration of the target, and the *u* and *v* axes represent the standard cosine and sine weighted integrals of the transient intensity $I(t)$:

$$u = \frac{\int_{t_1}^{t_2} I(t).\cos(\omega t).dt}{\int_{t_1}^{t_2} I(t).dt}, \qquad v = \frac{\int_{t_1}^{t_2} I(t).\sin(\omega t).dt}{\int_{t_1}^{t_2} I(t).dt}. \tag{1}$$

Where t_1 and t_2 define the start and end of the transient as well as the angular frequency $\omega = 2\pi/(t_2 - t_1)$. Pixel bins near the universal circle will have a dominant mono-exponential lifetime and we can filter those bins by defining a phasor 'radius', *r*, as the length of the vector from the phasor point to the (*u*,*v*) point (0.5, 0) at the center of the universal circle (distinct from the phasor magnitude that is the distance to (0,0)).

$$r = \sqrt{(u - 0.5)^2 + v^2}\,. \tag{2}$$

Referring to Figure 3 we see that a the FRET trajectory for small FRET efficiencies is almost perpendicular to the trajectory due to a concentration change, such that we can define an angle, θ, clockwise around the universal circle centered on (0.5,0), and a measure of average lifetime, $\tau(\theta)$ (See Appendix A)

$$\tau(\theta) = \frac{\sec(\theta) - \tan(\theta)}{\omega}. \tag{3}$$

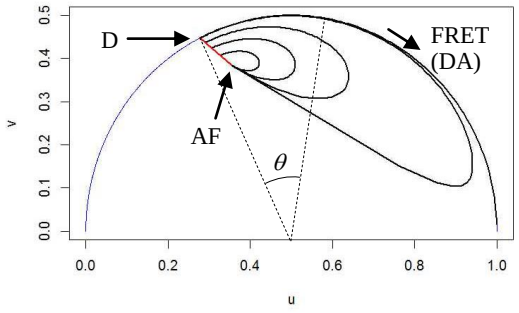

Figure 3. Phasor trajectories of fluorophores undergoing increasing FRET from the donor alone state (D, FRET Eff = 0%) to being in the presence of the acceptor (DA) and ultimately when the FRET Eff = 100% only the background autofluorescence (AF) can be measured. The u and v axes represent the standard cosine and sine weighted integrals of the transient that form the phasor diagram[32] and the universal semi-circle is also drawn for reference.

In the phasor analysis we are ignoring possible interfering effects such as a significant remaining constant background signal and prompt (IRF) width that are removed with the other fitting algorithms (MLE and Bayesian). These effects are not significant in our experiments.

3.4.4 Pixel bin filtering by lifetime

A filter that is specific to lifetime can be derived that can filter pixel bins that have a dominant lifetime in a certain lifetime range. Standard MLE multi-exponential fitting can be used but with lifetime parameters fixed it becomes a linear fitting problem that is robust at low photon counts. The fractional contribution of the target lifetime component can then be used to filter the pixel bins. The transient fluorescence intensity, *I(t)*, can be represented by the tri-exponential function:

$$I(t) = Z + A_1 e^{-\frac{t}{\tau_1}} + A_2 e^{-\frac{t}{\tau_2}} + A_3 e^{-\frac{t}{\tau_3}}. \quad (4)$$

where Z represents any background signal, A_i the component amplitudes and τ_i the component lifetimes. With the τ_i fixed we fit just for the Z and A_i and then the fractional contribution is defined thus:

$$f_i = \frac{A_i \tau_i}{\sum_j A_j \tau_j}. \quad (5)$$

By choosing the τ_i appropriately we can select for pixel bins with f_1 above some threshold, f_{th}. The primary component, τ_1, to be filtered for should be centered on the expected lifetime of the target fluorophore. The remaining τ_i may be chosen on the basis of expected AF components (Filter 1 below) or a band-pass filter may be created by choosing one lifetime higher and one lower than the target (Filter 2 below). For lifetime filtering pixels were binned until typically 10,000 counts were in each bin.

3.4.5 Cell pellet and tissue preparation

Cell pellet preparations offer the opportunity to have the controllability of a cell experiment but in a medium that is similar to a tissue section. MCF7 cells were cultured in DMEM supplemented with 10% FCS. Cells were transfected with Her2-GFP and Her3-GFP plasmids at ratio 3:1 using FuGene6 (Promega) according to the manufacturer's protocol, and cultured for 24 hours. Cells were fixed with 10% formalin for 5 hours and then processed overnight on Leica ASP300S and embedded into paraffin on Leica EG11508C. For staining cell pellets or tissue were cut (3 μm) and undergone same antigen retrieval procedure (BenchMark Ventana).

Antibodies: Anti-HER3 (B9A11) was purchased from Monogram Biosciences Inc., anti-HER2 (e2-4001+3B5) and anti-Her3 (2F12) were purchased from ThermoScientific Ltd. and directly labeled according to the manufacturer's protocol with Alexa546 (Her3) and Cy5 (Her2).

Plasmids: The HER2-mGFP construct was made by excision of HER2 from HER2-YFP (a kind gift from Selene Roberts, Rutherford Appleton Laboratory (RAL)) with XhoI and HindIII, and ligation into pEGFP-N1 (Clontech) containing an A206K mutation in the EGFP, enabling the EGFP to fold in a monomeric way. HER3-EGFP was also a kind gift from Selene Roberts.

3.4.6 Imaging parameters and number of frames

FLIM imaging was done on an 'open microscope' system similar to that described previously[1] at an imaging resolution of 256 by 256 and 256 time bins. Typically 100 to 200 frames were accumulated to gain sufficient photon counts. Filters suitable for imaging Alexa546 were used (Excitation filter: Semrock FF01-540/15-25; Beam Splitter: Edmund Optics 48-392 30R/70T; Emission filter: Semrock FF01-593/40-25). The imaging objective lens was a 20x 0.75 NA S Fluor (Nikon UK Ltd.) resulting in a field of view of 330 μm.

3.5 Results

It may be thought to be advantageous to bin all data from an image field into one transient in order to determine accurately the lifetime components present. This type of analysis is shown in Figure 4 where the result of applying the inverse Laplace transform algorithm to the combined data from a typical FLIM image is shown. Also shown is the result of fitting a tri-exponential model to the data in the TRI2 program. Both show that the combined image data fits sufficiently to a tri-exponential model but individual components cannot be precisely determined. This demonstrates that many more photon counts are required to resolve the Alexa546 lifetime (near 2.5 ns) and that combining all data from an image not only ignores tissue heterogeneity but also fails to offer a robust analysis when imaging in a reasonable time frame (limiting the counts available). We can also note that fitting multi-exponential models to pixel bins with far fewer counts should not be attempted.

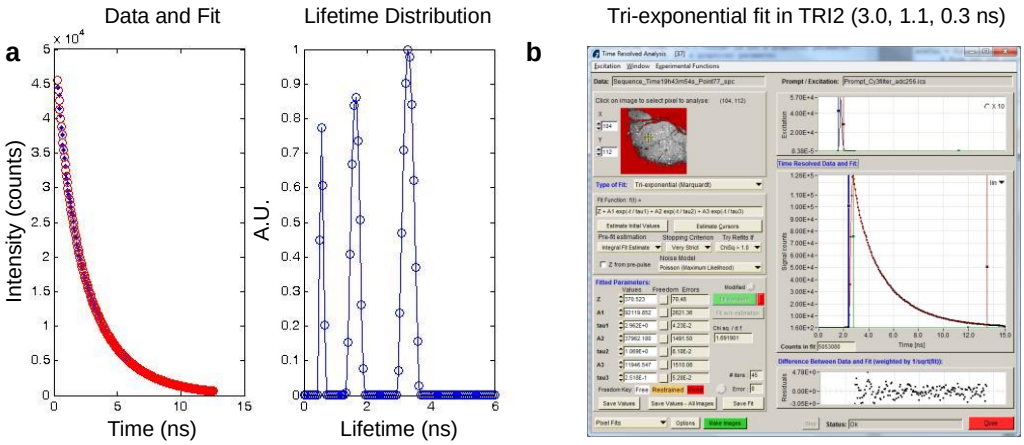

Figure 4. Time resolved data summed over a whole image acquired with typical imaging parameters (10 minutes acquisition, over 5 million photon counts in total) fitted with a model-free regularized inverse Laplace transform (a) and a tri-exponential model with MLE in TRI2 (b). (color in pdf version)

The results of applying the mono-exponential lifetime determination algorithms to the test image are presented in Figure 5 where the lifetime gradient produced by MLE, the Bayesian algorithm and the new phasor-based $\tau(\theta)$ can be seen. We should note that with MLE (Figure 5b) it is possible to measure a reduction in lifetime when the concentration of the donor changes in this test image and we move from the D region to the AF background region. With the other algorithms this effect is reduced due to the response of the Bayesian algorithm in the present of multi-exponential data and the insensitivity of $\tau(\theta)$ to concentration changes.

In Figure 5e, f, and g we see the behavior of the phasor and lifetime filters with this test image. The included areas (green/dotted) encompass the D region and exclude the AF region. Note that by changing the lifetime filter parameters (Filters 1 and 2 in e and f) we are able to tune the filter to include more or less of the DA region. This is beneficial when large lifetime changes from the D value are not expected and more specificity is desired.

Cell pellet preparations offer the opportunity to have the controllability of a cell experiment (i.e. to have chemically identical preparations, as far as biologically possible, that can be prepared as D or DA samples) but in a medium that is

similar to a tissue section (the pellets are sectioned and undergo the same paraffin embedding and mounting as tissue). D, DA and unstained samples (AF) were prepared and imaged by FLIM and the resulting intensity and lifetime images can be seen in Figure 6a. We can see here that with real data the phasor and lifetime filters exhibit the characteristics desirable in that they leave many of the D and DA pixels untouched but *exclude* almost all of the pixels from the unstained samples. Statistics from the 6 D and 6 AF samples can be seen in Figure 6b where it is clear that the filters reduce the effect of AF pixels in the lifetime by removing these pixel bins from the analysis.

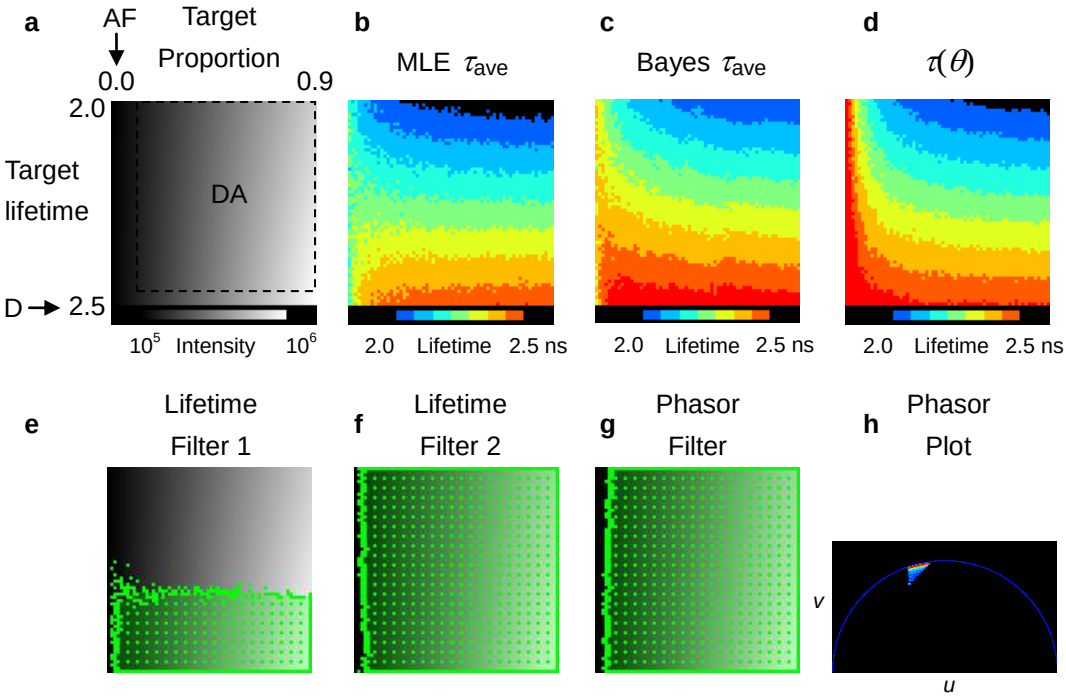

Figure 5. Results of applying the filters to the simulated test tissue. (a) Intensity image of the simulated lifetime data showing the horizontal gradient of target fluorophore proportion and the vertical gradient of target lifetime. Three areas are marked corresponding to the background autofluorescence (AF), the donor alone (D) and the FRET area where the donor is in the presence of the acceptor (DA). (b,c,d) Lifetime images determined by the MLE, Bayesian and phasor algorithms respectively. Quantized display lookup tables have been used for clarity in the printed version. (e,f,g) Green (dotted) areas correspond to the filtered areas of the test image for lifetime filter 1 (tri-exponential 2.5, 1.2, 0.3 ns, $f_{th} = 0.9$), lifetime filter 2 (tri-exponential 2.25, 3.5, 0.5 ns, $f_{th}=0.5$) and a phasor filter ($r_{th} = 0.45$). (h) The phasor plot of the test image showing the majority of pixels lying on the universal circle. (color in pdf version)

Finally, the effect of the filters on breast cancer tissue sections (from Guy's Breast Cancer Tissue Bank) is shown in Figure 7. In selected images from tissue microarrays prepared from archived paraffin embedded tissue we see how areas of the image containing irrelevant structures can be removed, or their area reduced compared to that of relevant tissue. In addition to this application to Alexa546 staining, successful results have also been achieved with Cy2 staining (Lifetime filter: 1.0 (target), 2.8 and 0.2 ns).

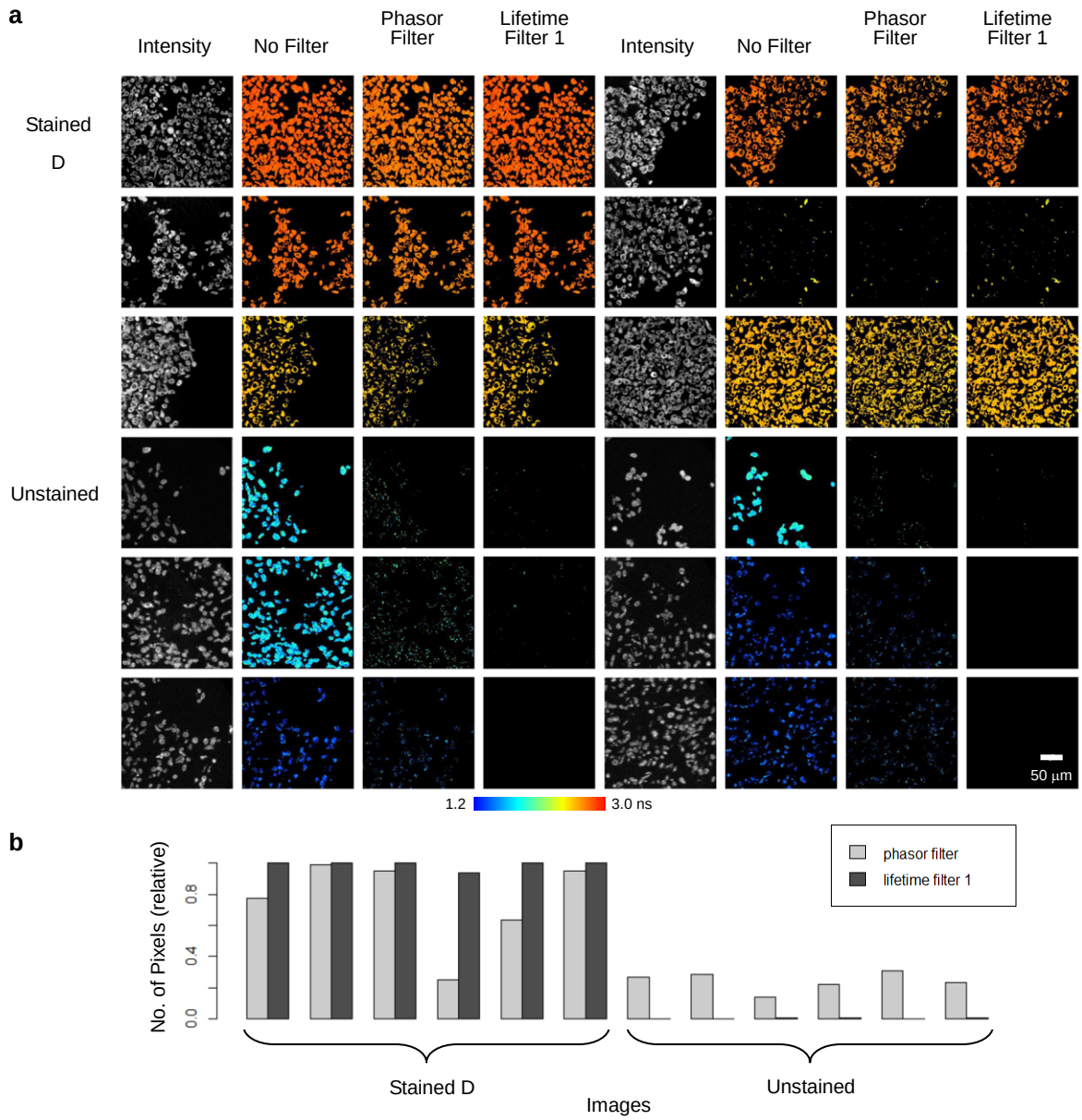

Figure 6. Application of the filters to FLIM images of cell pellets. (a) Intensity images and resulting lifetime images after applying a mono-exponential Bayesian fit (intensity thresholded), the same fit after a phasor filter (r_{th} = 0.47) and the same fit after the lifetime filter of type 1 (tri-exponential 2.5, 1.2, 0.3 ns, f_{th} = 0.85) for stained donor alone (D) and unstained cells. (b) Plot of the relative number of pixels that contributed to the average lifetime after the filter, compared to the total number when no filter is used. Note how the filters drastically reduce the number of auto-fluorescent pixels reducing their effect on the average lifetime. Intensity images have been linearly intensity scaled for clarity. (color in pdf version)

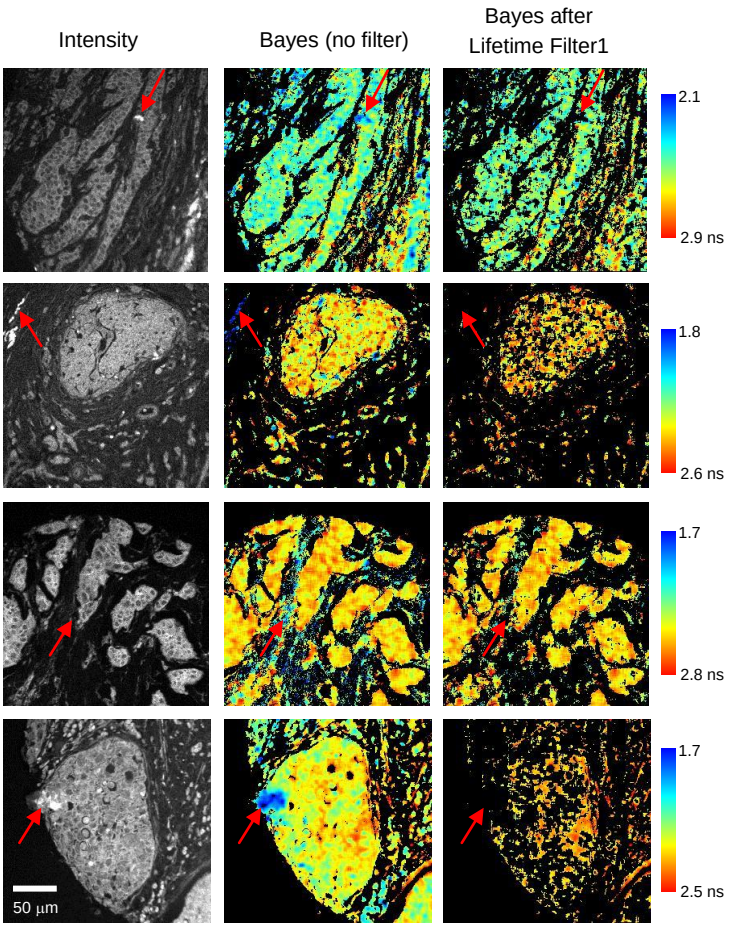

Figure 7. Example tissue FLIM images analyzed first with the Bayesian algorithm with no filter and then after the application of the lifetime filter (tri-exponential 2.5, 1.2, 0.3 ns, $f_{th} = 0.85$). Arrows indicate areas where the filter has been most visibly effective. Lifetime ranges are linear and optimized for clarity. (color in pdf version)

4. DISCUSSION

The open microscope methodology allows flexible and robust research microscopes to be built for a variety of purposes including radiation endstations and automated FLIM microscopes. The radiation endstations offer flexible microscope arrangements that physically fit with such an environment involving radiation shielding and other relevant requirements. Putting advanced and robotic microscope systems in that environment will enable novel experiments to be performed, aiding, for example, the investigation of DNA repair at early times following irradiation.

Moving forward with projects to detect protein interactions in tissue, we are now in a position to analyze large numbers of tissue sections in tissue microarray format with an open microscope. In this paper we presented developments in automated tissue segmentation by lifetime filtering that allow the automated removal of areas that are dominated by

interfering fluorescence (auto-fluorescence (AF), including endogenous and preparation induced fluorescence) that has a lifetime differing from the target donor fluorophore (e.g. Alexa546 or Cy2). We are particularly concerned with AF that has a lower lifetime than the target as this has the ability to give false FRET measurements by reducing the average lifetime through a change in target concentration. Lifetime Filter 1 has optimized parameters for this purpose based on tissue measurements (e.g. Figure 4); Filter 2 is a more general band-pass filter that includes a lifetime component longer than the target. AF with lifetimes equal or larger to the target will only act to reduce the FRET signal, so, although this is undesirable, it should not result in misled experimental findings. Average FRET values per imaged field of view (with an area >10,000 μm^2, say) should not be used for tumor characterization because tissue heterogeneity will result in undesirable areas being included (e.g. stromal tissue), and the necessity for extreme number of photon counts (>>10^7) needed to resolve the target from the AF components. We demonstrate segmentation via the lifetime filter that is not possible with intensity thresholds alone because of the variation in recorded intensity between the many tissue sections imaged. The method presented requires few photon counts (1,000 to 10,000) and is therefore applicable to small areas of pixels, thus preserving and accounting for tissue heterogeneity.

AKNOWLEDGEMENTS

We are indebted to J Prentice, G Shortland, K Kirkby, G Grime, M Merchant, and J C Jeynes and for distinct aspects of the work presented here. This work was supported by CR-UK (grants C133/A/1812 and C1519/A6906) and the King's College London-UCL Comprehensive Cancer Imaging Centre (CR-UK & EPSRC), and in association with the MRC and DoH as well as funded by the European Union Seventh Framework Programme (FP7, IMAGINT EC GRANT: 259881).

APPENDIX A

Assume the photo-physical system is multi-exponential with several components of unknown number, but is defined by lifetimes τ_i, and the amplitude fractions F_i $\left(\sum F_i = 1\right)$. The time-resolved fluorescence emission being determined by

$$I \propto \sum F_i . e^{-t/\tau_i} , \tag{A1}$$

in the presence of insignificant background. We can let our target fluorophore correspond to i=1, so in the D sample $\tau_1 = \tau_D$, in the DA sample $\tau_1 = \tau_{DA}$, and in the background F_1 is small. The intensity-based fractional contributions (integral or area under the curve) are given by:

$$f_i = \frac{F_i \tau_i}{\sum F_i \tau_i} . \tag{A2}$$

We treat our target fluorophore as a mono-exponential species (even when D and DA are mixed), and measuring τ_1 leads us to the *effective* FRET efficiency. This can be justified because we are only trying to derive a filter for the target fluorophore and treating it as two species (D and DA) overcomplicates with parameters that we can never hope to resolve. Also, analysis following the filter will be a mono-exponential fit, for robustness, and the determination of the effective FRET efficiency. Therefore, in this system where D and DA are treated as the same species, corresponding to τ_1, F_1 must remain constant when faced with a change in effective FRET efficiency, as this proportion of molecules remains

constant (the emitted intensity will change with FRET). The aim in the following paragraphs is to derive a phasor based approach to filtering those pixels where F_1 is large and also measuring the effective FRET efficiency from them. From experience we know that the FRET efficiency will be small so we can safely consider values up to 0.2. From the phasor trajectories for FRET (Figure 3) we see that it always initially moves to the right around the universal circle, for all starting values of F_1.

A phasor based filter can be easily made from the proximity to the universal circle. Pure mono-exponential phasors will appear on the circle with mixtures inside. If we make the assumption, backed by experimental data, that the tissue background will be a mixture and have no one strong component, we can assume that phasors lying near to the universal circle are high in F_1. The proximity to the circle circumference can be measured by the distance from the $(u,v)=(0.5,0)$ center point. Using this assumption that the phasor will be very near to the universal circle, we can derive a FRET measure based on the phasor FRET trajectory. In the phasor coordinate system (u,v), the phasor for the complex mixture is given by[37]:

$$u = \sum \frac{f_i}{1+\tau_i^2\omega^2}, \qquad v = \sum \frac{f_i\,\tau_i\,\omega}{1+\tau_i^2\omega^2}, \tag{A3}$$

where ω is the phasor angular frequency. We can define an angle, θ, that is the angle around the universal circle, given by

$$\theta = \arctan\left(\frac{u-1/2}{v}\right), \tag{A4}$$

which is completely general and defined for all values of (u,v). This will measure the progress around the initial part of the FRET trajectory. We need the function that expresses τ_1 in terms of θ in order to report some recognizable lifetime and FRET efficiency numbers. Substituting Equation A3 into Equation A4 we have

$$\theta = \arctan\left(\frac{\sum \frac{f_i}{1+\tau_i^2\omega^2} - 1/2}{\sum \frac{f_i\,\tau_i\,\omega}{1+\tau_i^2\omega^2}}\right). \tag{A5}$$

To proceed further we can use the fact that we have filtered the pixels such that f_1~1, and all other components are small and $\tau_{1=}\,\tau$. Then we can write

$$\tan(\theta) = \frac{\frac{1}{1+\tau^2\omega^2} - 1/2}{\frac{\tau\,\omega}{1+\tau^2\omega^2}} = \frac{1-\tau^2\omega^2}{2\tau\omega}, \tag{A6}$$

and we have the quadratic equation in τ

$$0 = \tau^2\omega^2 + 2\tau\omega\tan(\theta) - 1, \tag{A7}$$

with solutions

$$\tau(\theta) = \frac{-2\omega\tan(\theta) \pm \sqrt{4\omega^2\tan^2(\theta) + 4\omega^2}}{2\omega^2}$$
$$= \frac{-\tan(\theta) \pm \sqrt{\tan^2(\theta) + 1}}{\omega} \quad . \qquad \text{(A8)}$$
$$= \frac{\sec(\theta) - \tan(\theta)}{\omega}$$

REFERENCES

[1] Barber, P.R., Tullis, I.D.C., Pierce, G.P., Newman, R.G., Prentice, J., Rowley, M.I., Matthews, D.R., Ameer-Beg, S.M., and Vojnovic, B., "The Gray Institute 'open' high-content, fluorescence lifetime microscopes," J. Microscopy 251(2), 154–67 (2013).

[2] von Sonntag, C. [The Chemical Basis of Radiation Biology]. Taylor and Francis, London, (1987).

[3] Ward, J.E. "Nature of lesions formed by ionizing radiation". In DNA damage and Repair. Human Press, Totowa NJ, Vol. 2. (1998).

[4] Ward, J.F. "DNA damage and repair". Basic Life Science., 58, 403–415 (1991).

[5] Farah, K., Mejri, A., Hosni, F., Hamzaoui, A. H. and Boizot, B. "Formation and Decay of Colour Centres in Silicate Glasses Exposed to Gamma Radiation: Application to High-Dose Dosimetry", Current Topics in Ionizing Radiation Research, Dr. Mitsuru Nenoi (Ed.), ISBN: 978-953-51-0196-3 (2012).

[6] Levy, P. W. "Overview Of Nuclear Radiation Damage Processes: Phenomenological Features Of Radiation Damage In Crystals And Glasses," Proc. SPIE 0541, Radiation Effects on Optical Materials, 2 (1985); doi:10.1117/12.975356

[7] Kinner, A., Wu, W., Staudt, C., Iliakis, G. "Gamma-H2AX in recognition and signalling of DNA double-strand breaks in the context of chromatin." Nucleic Acids Res., 36, pp. 5678-5694, ISSN 0305-1048 (2008).

[8] Barnard, S., Bouffler, S. and Rothkamm, K. "The shape of the radiation dose response for DNA double-strand break induction and repair" Genome Integrity, **4**:1 (2013), doi:10.1186/2041-9414-4-1

[9] Paull, T. T., Rogakou, E. P., Yamazaki, V., Kirchgessner, C.U., Gellert, M. and Bonner, W. M. "A critical role for histone H2AX in recruitment of repair factors to nuclear foci after DNA damage" Current Biology, 10:886–895 (2000).

[10 Kashino, G., Prise, K.M., Schettino, G., Folkard, M., Vojnovic, B., Michael, B.D., Suzuki, K., Kodama, S., Watanabe, M. "Evidence for induction of DNA double strand breaks in the bystander response to targeted soft X-rays in CHO cells." Mutat. Res.,Vol. 556, pp. 209–215 (2004), ISSN 0027-5107.

[11] Prise, K.M., Pinto, M., Newman, H.C., Michael, B.D. "A review of studies of ionizing radiation-induced double-strand break clustering." Radiat Res, Vol. 156, pp. 572–576 (2001), ISSN 0033-7587.

[12] Kiefer, J. "Mutagenic effects of heavy charged particles." J Radiat Res (Tokyo) 43 Suppl: S21–S25 (2002).

[13] Folkard, M., Prise, K.M., Schettino, G., Shao, C., Gilchrist, S. and Vojnovic, B., "New insights into the cellular response to radiation using microbeams," Nuclear Instruments and Methods in Physics Research B, 231, 189–194 (2005).

[14] Folkard, M., Vojnovic, B., Gilchrist, S., Prise, K.M., and Michael, B.D. "The design and application of ion microbeams for irradiating living cells and tissues," Nuclear Instruments and Methods in Physics Research B 210,

302-307 (2003).

[15] Folkard, M., Vojnovic, B., Prise, K.M. and Michael, B.D., "The application of charged particle microbeams in radiobiology," Nuclear Instruments and Methods in Physics Research B, 188, 49-54 (2002).

[16] Grime GW. "A compact beam focusing and steering element using quadrupoles with independently excited poles." Nuclear Instruments and Methods in Physics Research, Section B: Beam Interactions with Materials and Atoms, 306, pp. 12-16 (2013).

[17] Kirkby, K.J., Grime, G.W., Webb, R.P., Kirkby, N.F., Folkard, M., Prise, K.M., and Vojnovic, B. "A scanning focused vertical ion nanobeam: a new UK facility for cell irradiation and analysis," Nuclear Instruments and Methods in Physics Research B 260, 97–100 (2007).

[18] http://www.surrey.ac.uk/ati/ibc/research/bio_medical/index.htm

[19] Merchant, M.J., Jeynes, J.C.G., Grime, G.W., Palitsin, V., Tullis, I.D.C., Barber, P.R., Vojnovic, B., Webb, R.P., and Kirkby, K.J., "A focused scanning vertical beam for charged particle irradiation of living cells with single counted particles," Rad. Res. 178, 182–190 (2012).

[20] Jares-Erijman, E.A., and Jovin, T.M., "Imaging molecular interactions in living cells by FRET microscopy," Curr. Opin. Chem. Biol. 10(5), 409–416 (2006).

[21] Lakowicz, J.R., [Principles of Fluorescence Spectroscopy] , Plenum Publishers, New York (1999).

[22] Ng, T., Squire, A., Hansra, G., Bornancin, F., Prevostel, C., Hanby, A., Harris, W., Barnes, D., Schmidt, S., et al., "Imaging Protein Kinase Calpha Activation in Cells," Science 283, 2805–2809 (1999).

[23] Wouters, F.S., Verveer, P.J., and Bastiaens, P.I., "Imaging biochemistry inside cells," Trends Cell Biol. 11(5), 203–11 (2001).

[24] Becker, W., [Advanced Time-Correlated Single Photon Counting Techniques] , J. A. W. Castleman, J. P. Toennies, and W. Zinth, Eds., Springer-Verlag (2005).

[25] Billinton, N., and Knight, A.W., "Seeing the Wood through the Trees: A Review of Techniques for Distinguishing Green Fluorescent Protein from Endogenous Autofluorescence," Analytical Biochemistry 291(2), 175–197 (2001).

[26] Tadrous, P.J., Siegel, J., French, P.M., Shousha, S., Lalani, E.-N., and Stamp, G.W., "Fluorescence lifetime imaging of unstained tissues: early results in human breast cancer," J. Path. 199(3), 309–317 (2003).

[27] Provenzano, P.P., Eliceiri, K.W., Yan, L., Ada-Nguema, A., Conklin, M.W., Inman, D.R., and Keely, P.J., "Nonlinear Optical Imaging of Cellular Processes in Breast Cancer," Microsc. Microanal. 14, 532–548 (2008).

[28] Fruhwirth, G.O., Fernandes, L.P., Weitsman, G., Patel, G., Kelleher, M., Lawler, K., Brock, A., Poland, S.P., Matthews, D.R., et al., "How Förster Resonance Energy Transfer Imaging Improves the Understanding of Protein Interaction Networks in Cancer Biology," ChemPhysChem 12(3), 442–461 (2011).

[29] Patel, G.S., Kiuchi, T., Lawler, K., Ofo, E., Fruhwirth, G.O., Kelleher, M., Shamil, E., Zhang, R., Selvin, P.R., et al., "The challenges of integrating molecular imaging into the optimization of cancer therapy," Integr. Biol. 3(6), 603–631 (2011).

[30] Colyer, R.A., Lee, C., and Gratton, E., "A novel fluorescence lifetime imaging system that optimizes photon efficiency," Microscopy Research and Technique 71(3), 201–213 (2008).

[31] Barber, P.R., Ameer-Beg, S.M., Gilbey, J., Edens, R.J., Ezike, I., and Vojnovic, B., "Global and pixel kinetic data analysis for FRET detection by multi-photon time-domain FLIM," Proc. SPIE 5700, 171–181 (2005).

[32] Digman, M.A., Caiolfa, V.R., Zamai, M., and Gratton, E., "The Phasor Approach to Fluorescence Lifetime Imaging

Analysis," Biophys. J. 94(2), L14–16 (2008).

[33] Barber, P.R., Ameer-Beg, S.M., Gilbey, J., Carlin, L.M., Keppler, M., Ng, T.C., and Vojnovic, B., "Multiphoton time-domain FLIM: Practical application to protein-protein interactions using global analysis," J. R. Soc. Interface 6, S93–S105 (2009).

[34] Laurence, T.A., and Chromy, B.A., "Efficient maximum likelihood estimator fitting of histograms," Nat. Meth. 7(5), 338–339 (2010).

[35] Rowley, M., Barber, P.R., Coolen, A.C.C., and Vojnovic, B., "Bayesian analysis of fluorescence lifetime imaging data," Proc. SPIE 7903, 74 (2011).

[36] Provencher, S.W., "CONTIN: A general purpose constrained regularization program for inverting noisy linear algebraic and integral equations.," Comput. Phys. Commun. 27, 229 (1982).

[37] Colyer, R.A., Siegmund, O.H.W., Tremsin, A.S., Vallerga, J.V., Weiss, S., and Michalet, X., "Phasor imaging with a widefield photon-counting detector," Journal of Biomedical Optics 17(1), 016008–1 (2012).